# Primary Electron Transport and Losses in a Ring-Cusp Discharge Chamber

**IEPC-2009-156**

*Presented at the 31st International Electric Propulsion Conference,*
*University of Michigan • Ann Arbor, Michigan • USA*
*September 20 – 24, 2009*

Aimee A. Hubble[*] and John E. Foster[†]
*University of Michigan, Ann Arbor, Michigan, 48109, USA*

**Electron current density profiles were obtained in the region above a magnetic cusp in a 20 cm partial conic ring cusp ion thruster discharge chamber to study electron collection mechanics in the absence of gas flow and plasma production. This represents the first stage in a series of experiments aimed at better elucidating collection physics at the magnetic cusps during discharge chamber operation. From these current density maps, primary electron transport through the cusp could be visualized. Attenuation coefficients and loss widths as a function of probe distance above the anode were calculated from the current density data. Floating emissive probe measurements were also made in the region of the magnetic cusp to determine the degree of potential distortion that occurs during electron transport. The potential profiles obtained with the probe were compared to the vacuum potential profile using a commercially available electrostatic solver.**

## I. Introduction

THOUGH much progress has been made in the study of magnetic cusps in plasma sources, the physics of plasma losses at magnetic cusp surfaces in multipole ion sources remains a fundamental yet poorly understood problem[1-7]. Effective loss area at the wall in these sources controls discharge ionization performance, efficiency, and stability[3,8,9]. This work makes an effort to better understand the mechanics of plasma losses at magnetic cusps and, with this knowledge, assigns an effective loss area that can be used to provide a general accounting of plasma particle losses to the wall[1,5,10]. Once determined, the effective loss area parameter can be used to simplify the modeling and design of ion source discharge chambers featuring multipole containment.

A ring-cusp discharge chamber utilizes a series of magnetic rings of alternating polarity to create a magnetic circuit that increases the containment path length of the primary electrons[11,12,13]. It is particularly important to increase the path length of the primary electrons since they drive ionization in the chamber[2,9,11,14-16,18]. The magnetic topology should ideally ensure that each primary electron as well as the energetic electrons in the tail of the plasma electron energy distribution undergoes at least one ionization before being collected at the anode. This is accomplished by placing constraints on the electron's trajectory and limiting the collection area such that most of the particles are lost to the narrow regions defined by the magnetic cusps and not the entire anode surface. The size of the cusp regions depends on the magnetic circuit geometry while the effectiveness of such a geometry at confinement is dependent on collisional diffusion.

Many studies have investigated the magnetic cusps[5,10,19-21]. Limpaecher and MacKenzie[12] showed that the use of point cusp geometry improves both ion source plasma density and plasma uniformity, and since then improvements in permanent magnet configurations have led to the ring cusp geometry that is used in present-day thrusters[22,23]. It was not the magnetic field that gave rise to the density improvement in these sources, rather it was the improved confinement of the primary electrons[18,24]. In order to improve confinement time, research focused attention on the

[*] Graduate Student Research Assistant, Department of Nuclear Engineering and Radiological Sciences, aacovert@umich.edu.
[†] Associate Professor, Department of Nuclear Engineering and Radiological Sciences, jefoster@umich.edu.

so-called loss width of the cusp, which is related to the effective loss area that the magnetic cusp projects to the plasma. Hershkowitz[19] and others[1,4,6] have determined this width to be related to the hybrid radius. However, previous work has suggested that the collection width at the anode surface does not singlehandedly determine the true effective loss area[25]; that is, the area established by the loss width at the wall multiplied by the bulk plasma density may not be a good measure of particle loss rates. Indeed, previous work has shown considerable attenuation in particle flux as its transported to the wall through the magnetic cusps[25]. This would suggest that rather than a loss area determined at the wall, a transmission coefficient associated with the magnetic cusp might be a better measure of particle losses to the wall. This transmission coefficient is expected to be species dependent.

A 20 cm partial conic discharge chamber featuring four samarium-cobalt permanent magnet rings in a ring cusp configuration[22] was designed and constructed to study plasma losses at the anode in ion thrusters. In previous work[25], preliminary Langmuir probe measurements were made over one of the magnet rings by sweeping a translatable Langmuir probe across the magnet surface. In this work, we focus specifically on primary electron transport to the chamber walls. This is achieved by operating the discharge chamber without any gas flow. Primary electron transport is important in that it accounts for the majority of the ionization rate. The primary electron only tests and measurements have been refined through the use of an improved filament cathode and a high-resolution 3-axis motion control system.

In this work, the 20-cm discharge chamber is operated in the limit of zero gas flow and a base chamber pressure on the order of $10^{-5}$ Torr such that the chamber is populated almost entirely by primary electrons. A translatable Langmuir probe is used to interrogate the cusp region above an arbitrarily selected magnet ring. Complementary potential measurements are made with a translatable floating emissive probe. The potential measurements are compared with vacuum potential data obtained using a commercially available electrostatic solver. This work differs from previous work in that it presents a full 2-D map of the current density over the cusp region and compares this to potential measurements, giving a more complete picture of primary electron transport through the magnetic cusp.

This work is part of an ongoing effort to obtain a fundamental understanding of the role of the magnetic circuit on discharge efficiency. The ultimate goal is to use the knowledge gained to design efficient discharge chambers based on a fundamental understanding of the dependence of ionization on primary electron trapping and plasma electron collection at and between magnetic cusps. Such knowledge is also expected to add physical significance to current design rules particularly those regarding closure of magnetic contours near the anode wall[26]. From the magnetic circuit, particle losses can be determined which will allow for the computation of discharge conditions and efficiency. Then, by modifying the magnetic circuit, one can quickly optimize expected discharge performance in a straightforward fashion. The particle losses determined through this work will be incorporated into an energy and particle balance model like the one proposed by Lieberman[27] and modified for ion thrusters by Goebel[17].

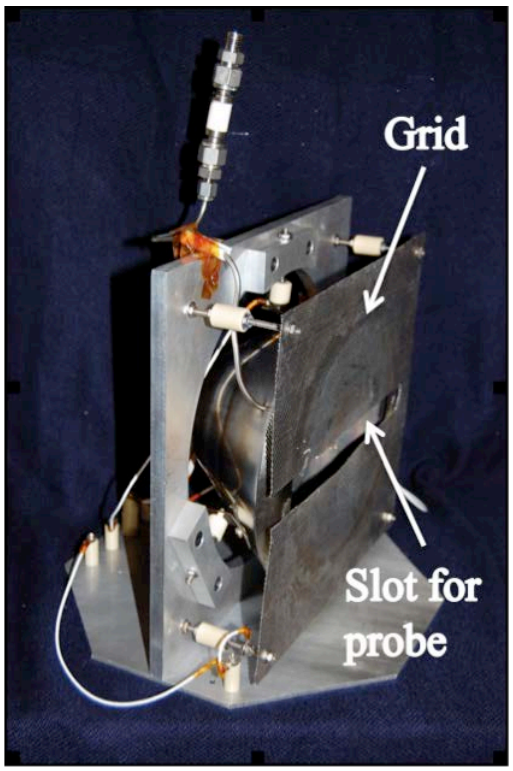


**Figure 1: Discharge chamber with grid and aluminum mounting plate. A slot was cut into the grid to allow the probe to interrogate the cusp region.**

## II. Experimental Setup

In previous work, a semi-conical discharge chamber was designed and built[25]. The discharge chamber features four samarium-cobalt permanent magnet rings. It is 20 cm in diameter at the exit plane and 10 cm long. The mild steel discharge chamber body and the magnet rings form the thruster anode. A tungsten filament fashioned from 0.5 mm wire was used as the thruster cathode. The filament is coated in R500 coating to improve emission and is electrically isolated from the anode using ceramic standoffs. A stainless steel grid was mounted at the exit plane using ceramic standoffs. For these experiments, the grid was allowed to float. The discharge chamber is electrically

isolated from an aluminum mounting plate and the entire setup is placed in a vacuum chamber. A picture of this setup is provided in Figure 1, and a cross-sectional schematic of the discharge chamber is given in Figure 2.

Two DC power supplies are used to operate the source. The first drove heating current through the filament and the second biased the anode at a positive voltage relative to the filament. Three probes were used in this experiment. A fixed Langmuir probe was mounted near the center of the discharge chamber to take bulk region measurements using an automated probe data acquisition system. A second Langmuir probe was used to measure current density across the magnet rings. This probe is pictured in Figure 3. This planar probe has a 1 $mm^2$ tantalum collection surface and is mounted on a macor extension arm. The extension arm connects to a three-axis motion control system. The "L" shape of the probe is intended to prevent shadowing caused by the probe body, which might block particles from reaching the cusp. The cusp probe was operated in the area above the third magnet ring, shown in Figure 2. Probe voltage was supplied by a DC power supply and an electrometer was used to record the probe current. Cusp probe currents were typically on the order of $10^{-7}$ A. Measurements were made with a resolution of 0.1 ± 0.01 mm parallel to the magnet surface over a 1.5 cm interrogation track. The measurements are repeated up to 11 mm above the anode surface, with a vertical step of 1 mm for a two-dimensional array of current density data, 1,650 data points in all. The result is a high-resolution current density map of the cusp region.

Measurements were also made utilizing a floating emissive probe[28]. The probe filament consisted of $6*10^{-3}$ cm diameter tungsten wire that connects to the emissive probe circuit through copper lead wires. A diagram of the probe is given in Figure 4. Figure 5 shows a photograph of the source with emissive probe and cathode in operation. The probe had an "L" shape similar to that of the cusp Langmuir probe and was connected to a macor extension arm that attached to the positioning system. The emissive probe was translated over the same magnetic cusp region interrogated by the planar Langmuir probe with identical spatial resolution. Uncertainty in probe measurements was on the order of nA for Langmuir probe data and mV for emissive probe data. Finally, a schematic of the experiment is given in Figure 6.

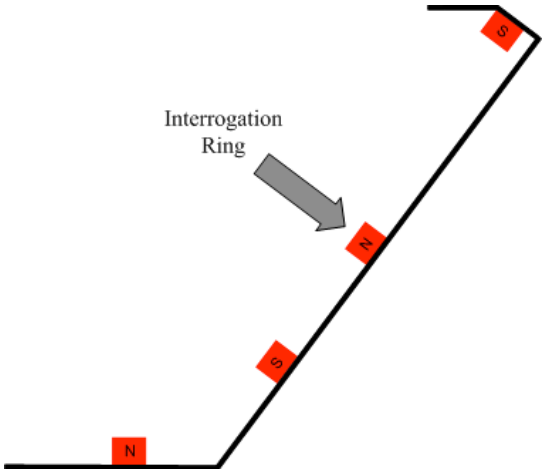


**Figure 2: Schematic of discharge chamber (radial cross section shown). Arrow indicates the magnet ring that was the subject of experiments.**

**Figure 3: Translatable Langmuir probe and macor extension arm**

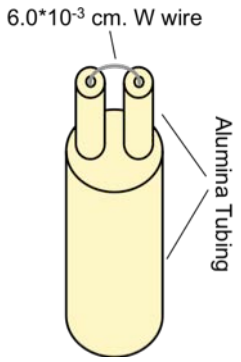


**Figure 4: Emissive probe diagram**

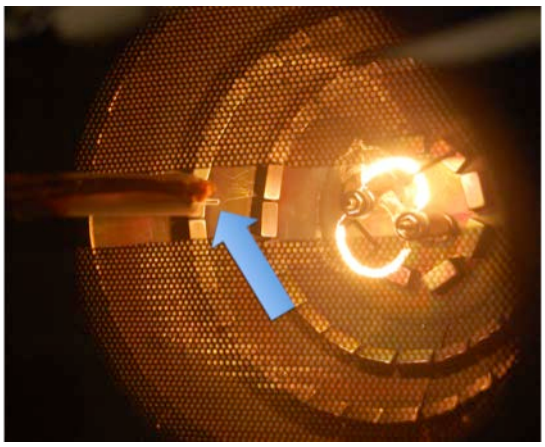

**Figure 5: Emissive probe and cathode in operation. The arrow points to the probe tip.**

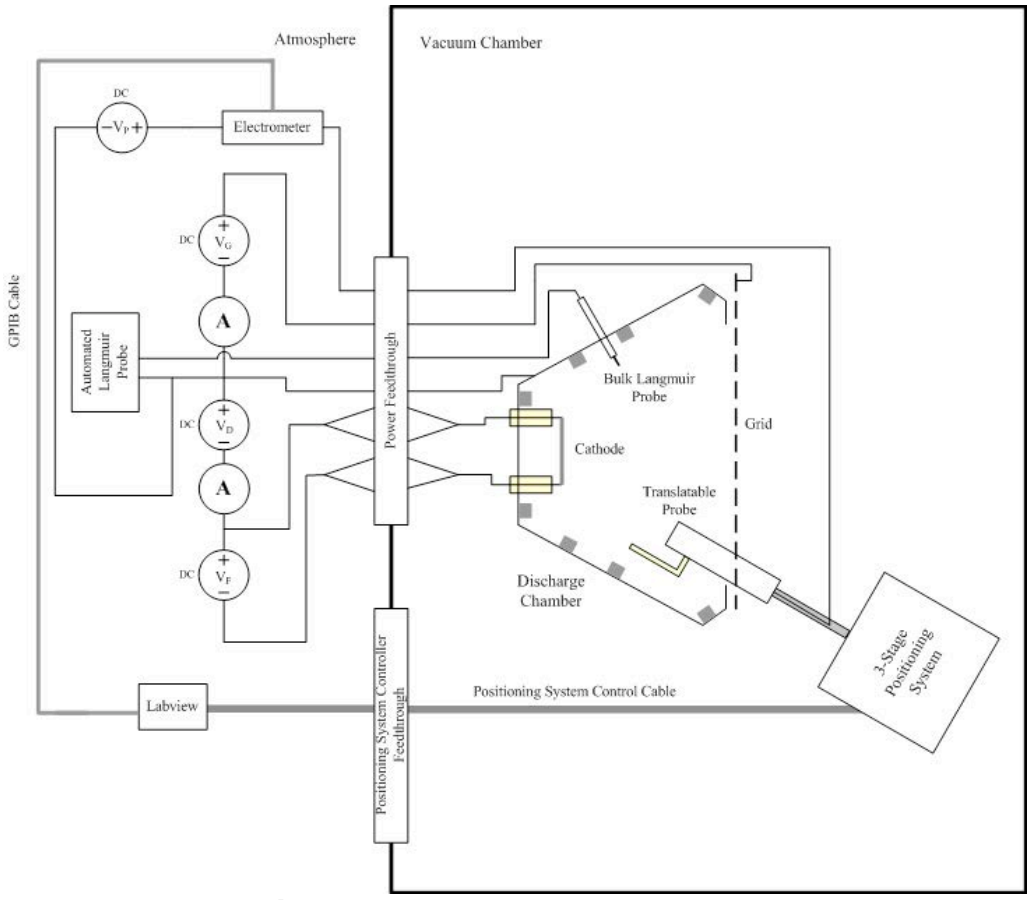


**Figure 6: Experiment schematic**

## III. Data Analysis

### A. Bulk Probe Data

A fixed Langmuir probe was placed near the center of the discharge chamber. This probe collected IV curves using an automated Langmuir probe system. This data is used to determine the energy and density of the primary electrons. A sample curve collected at 3.0 mA filament emission current is shown in Figure 7. As can be seen in Figure 7 the current does not go negative, which is consistent with the lack of appreciable ion density in the discharge chamber. The first derivative of the smoothed curve is plotted on top of the IV trace. A knee can be seen around 0 V, where there is a drop in the first derivative. Following the trace backwards, both probe current and its first derivative go to zero around -50 V, giving us an approximate primary electron energy of 50 eV. This corresponds to the discharge voltage drop between the cathode and anode, as expected.

To approximate the primary electron density at the location of the fixed probe Equation 1 is used:

$$n = {}^{I_e}\!/_{qAv} \tag{1}$$

where A is the cross sectional area of the cylindrical probe and v is the velocity of the electrons, given by $e\Phi = mv^2/2$. In each current case we obtain an approximate density on the order of $10^6$ #/cm$^3$. Interestingly, density in the bulk does not increase linearly with emission current; rather, the increase is sub-linear. Apparently at these pressures, the majority of the emitted electron current ends up trapped along field lines near the anode. This is consistent with a fairly high-direction electron beam with few scatters. The small increases in density that are

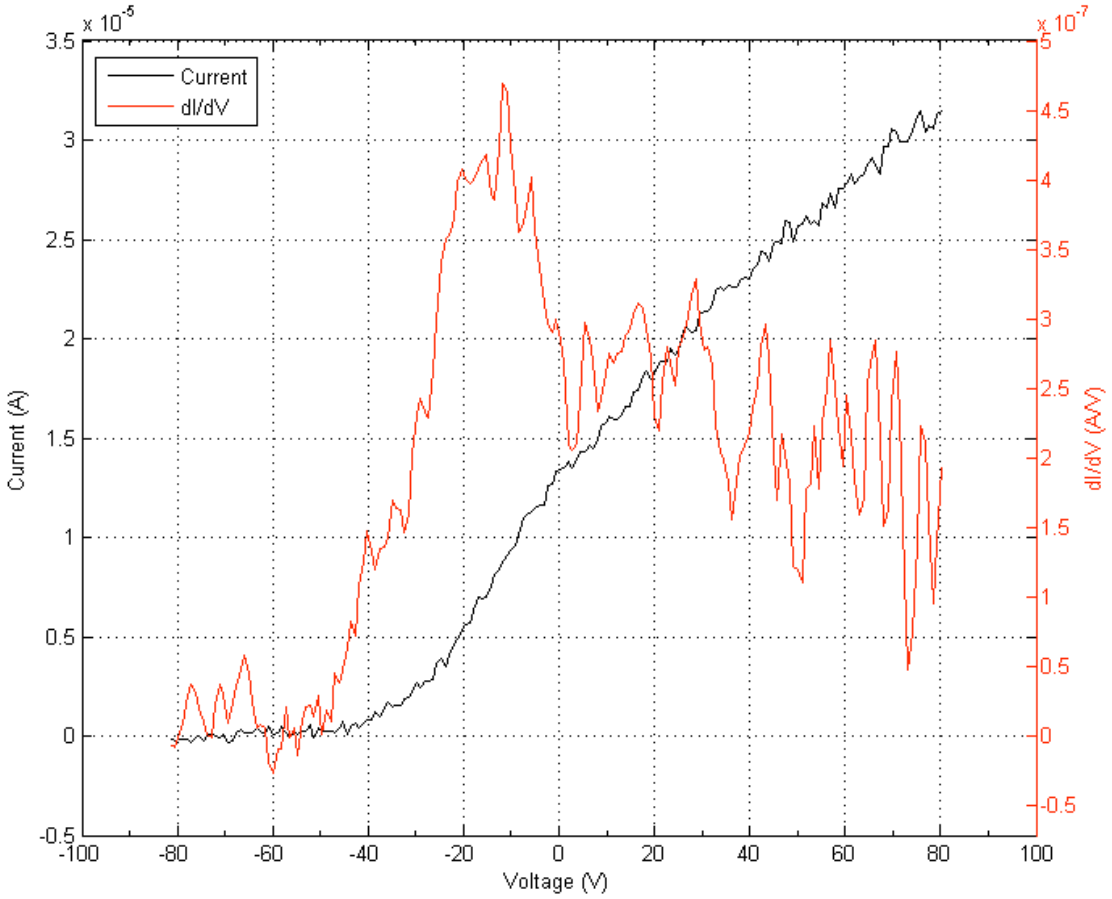


**Figure 7: Bulk probe IV trace for 3.0 mA case (black). First derivative of smoothed IV trace (red).**

observed with increasing emission current are likely a consequence of either electron scattering/reflection from cusps or localized residual ionization taking place along field lines near the anode surface. This peripheral plasma ultimately diffuses outward toward the central regions of the discharge chamber via cross-field diffusion processes. This would effectively reduce the rate of density increases with emission current. Radial density profiles and inferred diffusion coefficients are left to future work.

### B. Langmuir Probe Cusp Data

Spatial electron probe current profiles at the cusp were obtained for three cases: a low discharge current case (0.5 mA), a moderate discharge current case (1.3 mA) and a high discharge current case (3.0 mA). The low current case is presented in Figure 8, which shows a contour plot of the current collected by the probe across the interrogation area. Red indicates intense current flow on axis. The gray box below the x-axis represents the location of the magnet ring. A clearly defined funnel-shaped cusp is observed in the region above the magnet, however it is obvious that there is more current collected on the upstream filament facing (left hand side) side of the cusp, than on the downstream grid facing side. This effect is even stronger in the moderate and high current cases, presented in Figures 9 and 10, respectively. As can be seen in these figures, the center of the cusp is displaced from the exact center of the magnet. This may be because the magnet cusp itself has some finite width at the anode surface. That is, there is a region of maximum magnetic field near the center of the magnet, but the field is quite strong across the entire magnet surface and so electrons moving toward the cusp from the upstream portion of the chamber may be collected before they reach the magnet centerline. The center of the cusp appears to shift as discharge current increases. This may be the result of electrostatic effects as the left hand side of the cusp becomes loaded with electrons and

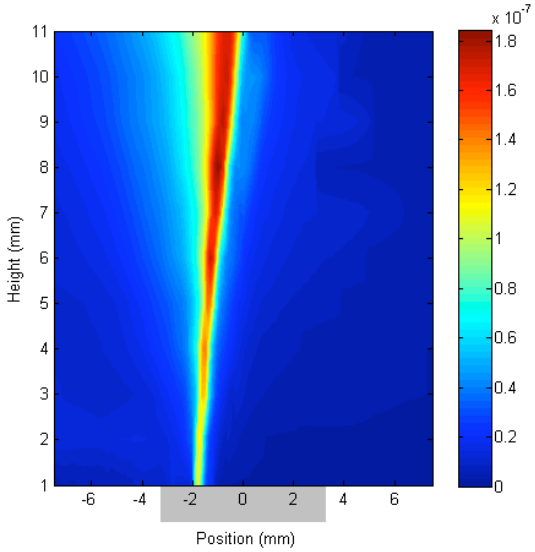


**Figure 8: Current density (A) profile in the cusp region at 0.5 mA discharge current.**

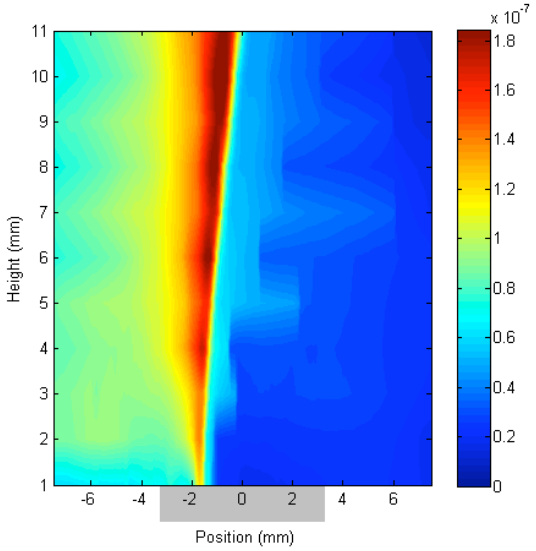


**Figure 9: Current density (A) profile in the cusp region at 1.3 mA discharge current.**

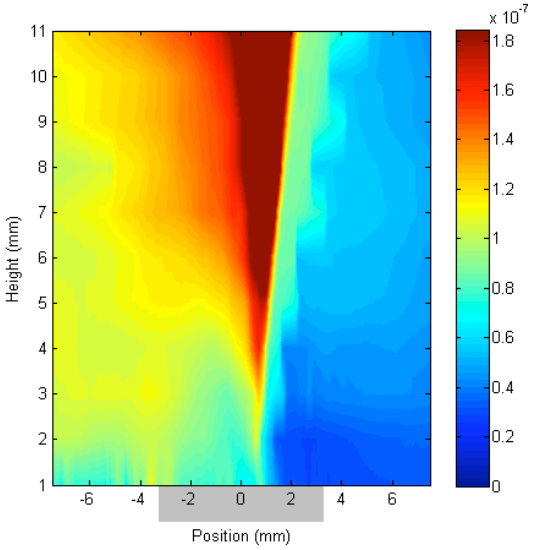


**Figure 10: Current density (A) profile in the cusp region at 3.0 mA discharge current.**

collection is pushed downstream. This offset will be investigated further in future work. In all three cases there appears to be much more current on the upstream side of the cusp than on the downstream side. In this case, the electrons appear to be loading the magnetic lobe between the second and third magnet rings. These rings are closest to the cathode. By line of sight argument, it is expected that the most upstream rings will capture the primary electrons and in the absence of an appreciable collision frequency as is the case in this work, the trapped electrons cannot readily diffuse to the other side of the cusp.

All three data sets are shown in Figure 11 in a side-by-side surface plot to show how the current peak shape in the cusp region shown in changes as a function of distance above the magnet. Note that the three cases are plotted on

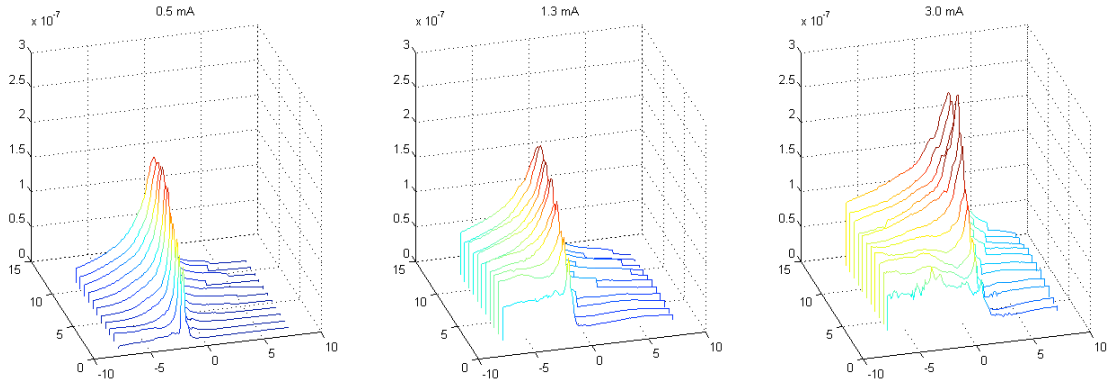


**Figure 11: Current density (A) profiles for 0.5 mA, 1.3 mA, and 3.0 mA discharge current cases.**

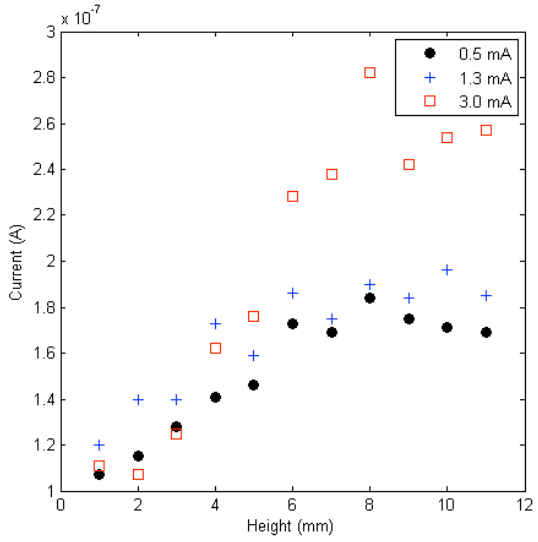


**Figure 12: Cusp center current (A) as a function of probe height.**

the same scale for comparison and all exhibit distinct asymmetry. Similar asymmetry in which increased current was observed in the upstream portion of the cusp, was observed in previous work[25]. The maximum current in each horizontal sweep is plotted as a function of height in each current case in Figure 12. This is expected to represent the current along the cusp centerline. Current saturation occurs around 6 mm above the anode surface, after which point current remains largely constant. This knee appears to be associated with the effective boundary of influence of the magnetic cusp, separating the cusp region from the bulk plasma region.

To better understand this data, it is useful to compare observed spatial behavior with magnetic field behavior predicted in the region using a commercially available magnetostatic solver. A cross-section of the discharge chamber and the corresponding magnetic field vector plot is shown in Figure 13. What we observe in the probe current plots is that the field lines between the second and third magnet rings appear to be loaded with electrons (as inferred from the upstream portion of the cusp data at ring 3), while relatively few of the primaries seem to orbit the field lines between the third and fourth rings. To fully confirm this, the full region between the second and third magnet region as well as the region between the third and fourth magnet ring will need to be interrogated, a task left for future work. As a result of the apparent loading of the field lines between the second and third rings, most of the current collected at the third ring occurs on the upstream side of the cusp. This result is not unexpected when considering the B-field plot shown in Figure 13. Electrons emitted by the filament are more likely to be collected at rings 2 and 3 due to the large magnetic lobe between those two rings. Owing to the absence of collisions with neutrals and ions in this vacuum case, the electrons cannot reach the far field lines; as a result, we observe a region of relative emptiness in the cusp. This loading may also account for the displaced cusp current profiles discussed in figures 8-10. The fact that the current profile is better centered over the center of the magnet at the higher current case is

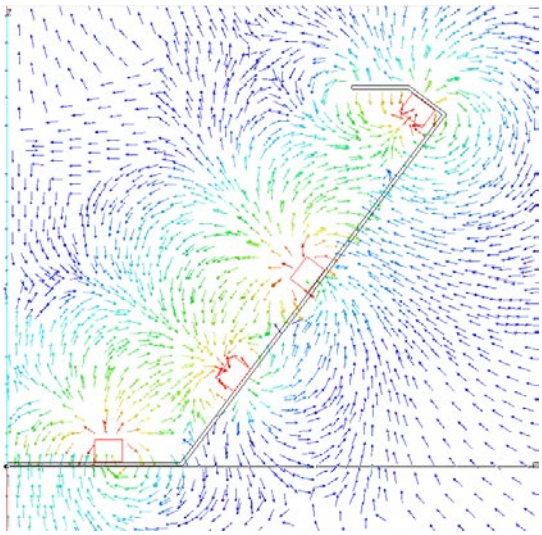

**Figure 13: Cross section of discharge chamber and calculated magnetic field vector plot. Red arrows correspond to a field strength of 3 kG and blue arrows correspond to 30 G.**

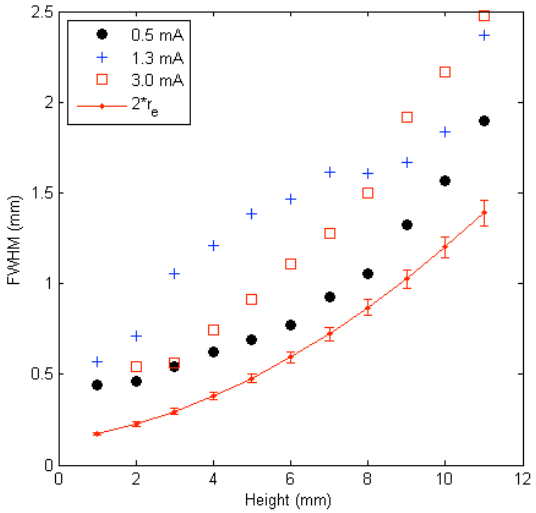


**Figure 14: FWHM versus probe height above the magnet surface for all three discharge current cases. $2*r_e$ is plotted for comparison.**

likely a consequence of the presence of a nontrivial ion population produced at the higher discharge currents. Electron ion collisions and charge separation field in the cusp region can give rise to diffusion of electrons across the field lines. The presence of plasma electrons would also tend to expand the cusp region. These collisonal effects are currently under investigation. Collisions appear to play a significant role in dispersing electrons throughout the discharge chamber, however too many collisions will increases particle losses to the walls. There is likely an ideal gas pressure at which electrons are well contained between the cusps and local peripheral ionization can take place there[13].

### C. Leak Width and Total Current in Cusps

The full width half maximum (FWHM) of each interrogation track is calculated and plotted versus probe height for each current case in Figure 14. The FWHM is determined by finding the width of the profile at the halfway point between the baseline current and the maximum current for each horizontal sweep. Assuming a primary electron temperature of 50 eV and measuring the magnetic field as a function of height above the anode, the Larmor radius of the primary electrons is calculated. This loss width near the anode wall is compared with twice the electron Larmor radius, the characteristic loss width scaling in this case, in Figure 14. The error bars indicate uncertainty in the magnetic field measurement. The estimated leak widths compared favorably magnitude and trend wise with the calculation. In all cases the experimentally obtained values were larger, which may be due to the finite width of the cusps or electrostatic effects Agreement tended to depend greatly on the discharge current. The discrepancy between twice the electron Larmor radius and experimental data increases with increasing discharge current suggesting space charge or sheath effects, and also indicates an increase in density with discharge current.

It is of interest to determine the amount of current that is crossing each of the horizontal interrogation tracks. By integrating the probe current over each interrogation track, a parameter that is proportional to this value can be obtained using the trapezoid rule over each of the sweeps parallel to the cusp. These integrations were obtained in order to determine how much of the current entering the mouth of the cusp actually ends up at the anode and are plotted for each of the current cases in Figure 15. The plot gives a measure of attenuation at a given height above the cusp relative to that at the mouth. Based on the data in Figure 15, the 11 mm starting interrogation height appears to reasonably represent input flux. As can be seen for currents above 6 mm, the integrated current (in units of A*mm) is essentially flat suggesting at distances above 6 mm, one is sampling the edge of the bulk plasma. The location of this boundary knee is consistent with the axial cusp current knee as well. As can be seen here in Figure 15, the rates of attenuation have similar slopes at similar heights. There appears to be a weak knee in all cases below which the rate of attenuation appears to increase. This occurs between 5 and 6 mm. Again, this is likely the transition between the bulk plasma and the cusp region of influence. This location is consistent with the significant gradient change observed in the current density profiles shown in figures 8-10. Physically, the change in attenuation is likely related to the loss cone associated with the magnetic cusp. Future work will investigate the loss cone based on real B field data at the cusp.

The degree of attenuation can be approximated by comparing the integrated current calculated at 11 mm above the anode to 1 mm above the anode. This gives transmission coefficients for each discharge current case, which are presented in Table 1 below. Since the closest interrogation occurred at 1 mm above the anode surface, these coefficients are not exact but are expected to give a good approximation of transmission through the cusp. The amount of electron transmission through the cusp increases dramatically with discharge current, suggesting that electrostatic effects may begin to play a role in collection once the field lines become saturated with electrons. It should also be pointed out that at the higher emission currents, increased ionization of the background gas is possible leading to the formation of plasma electrons which scatter more readily into the anode[9,12,29]. In any event, in vacuum-like conditions (the 0.5 mA case), transmission of primaries through the cusps is quite low. This coefficient should be a function of magnetic circuit layout as well as plasma conditions. This sensitivity is the subject of future work.

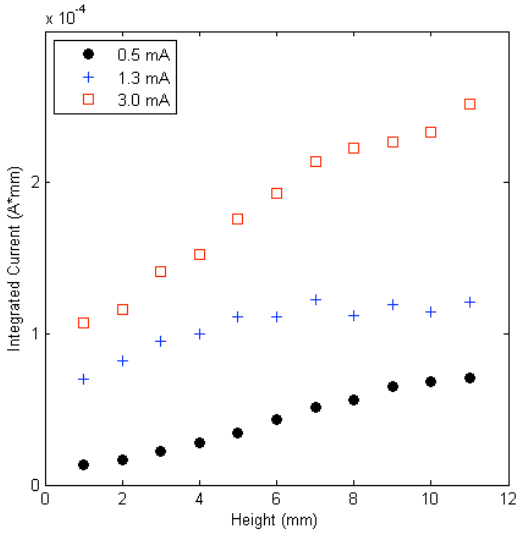


**Figure 15: Integrated current (A*mm) versus probe height above the magnet surface for all three discharge current cases.**

| Discharge Current (mA) | Transmission coefficient |
|---|---|
| 0.5 | 0.18 |
| 1.3 | 0.58 |
| 3.0 | 0.42 |

**Table 1: Transmission coefficients for each discharge current case**

### D. Emissive Probe Cusp Data

An attempt was made to use an emissive probe to assess electrostatic effects caused by trapped electrons in the cusp. The probe measurements are expected to give a qualitative measure of potential variations in the cusp region. Emissive probe potential data was collected in the cusp region in the low-current (0.5 mA) and moderate-current (1.3 mA) cases. This data is presented in Figures 16 and 17, respectively, which shows a contour plot of the potential in the cusp region. As before, the gray box below the x-axis represents the location of the magnet ring (azimuthal symmetry, rotation into the page). In both cases, the magnetic cusp tended to be more or less equipotential on each side of the cusp. On the upstream side (left side of the plot), they are quite close to the filament potential. On the downstream side (right side of the plot), they are closer to the anode potential. There is also a very distinct equipotential line along the cusp centerline, extending up into the bulk. These plots can be compared to the vacuum potential, calculated using a commercially available electrostatic solver. In the vacuum limit it is expected that the entire cusp region should be very close to the anode potential. This is indeed the case as depicted in Figure 18. This is the case also on the downstream side of the cusp when electrons are present as shown in Figure 16, suggesting that there are very few electrons that make it to the far field lines. This is also consistent with cusp current density data. This indicates a very large sheath in the

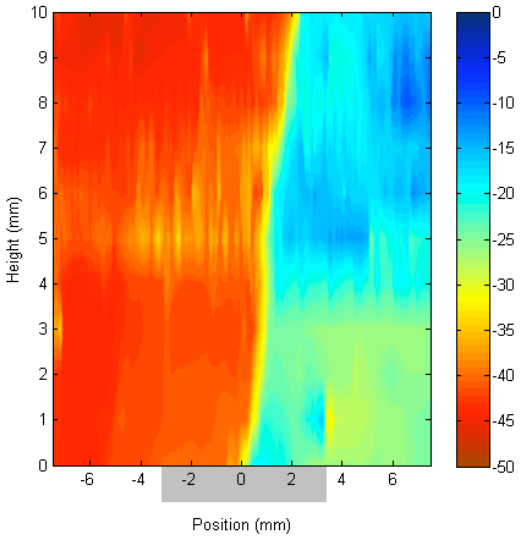


**Figure 16: Emissive probe data (V) for 0.5 mA discharge current case**

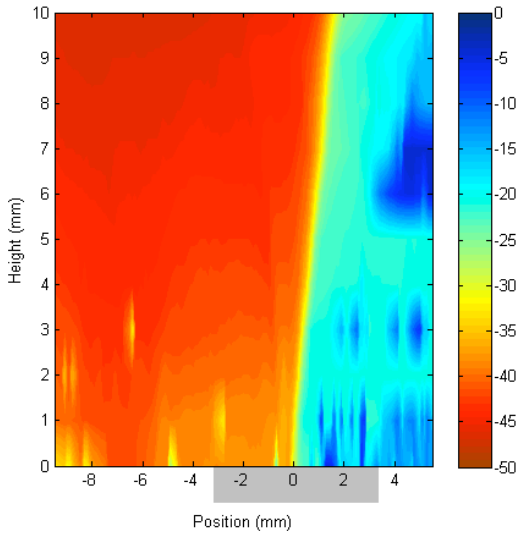


**Figure 17: Emissive probe data (V) for 1.3 mA discharge current case**

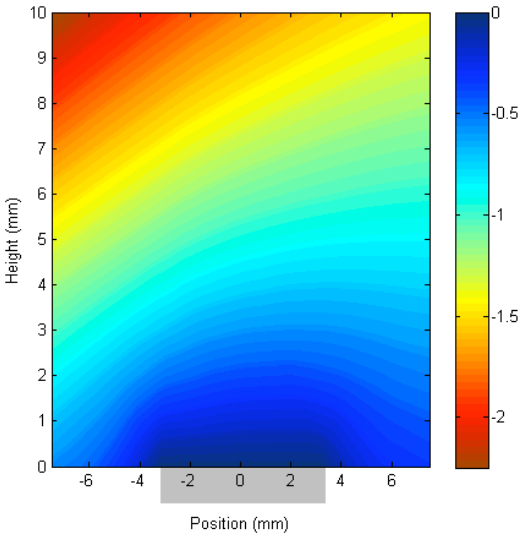


**Figure 18: Vacuum potential.**

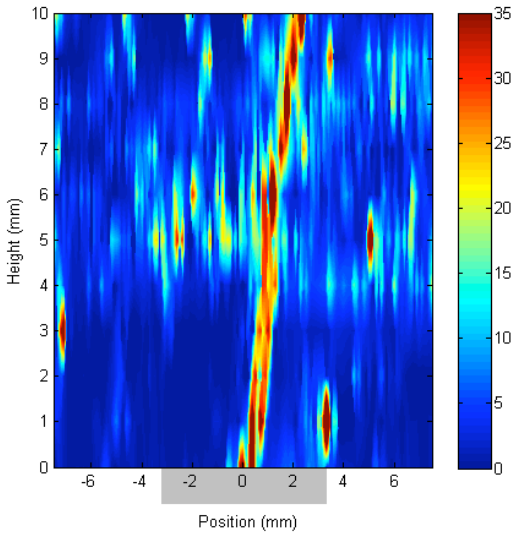


**Figure 19: Calculated electric field data (V/mm) for 0.5 mA discharge current case.**

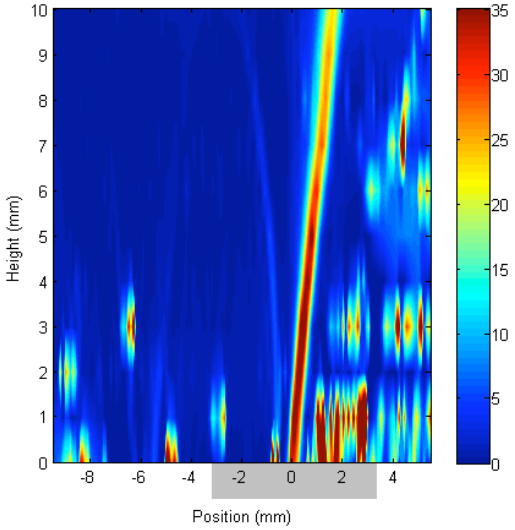


**Figure 20: Calculated electric field data (V/mm) for 1.3 mA discharge current case.**

upstream portion of the anode region around the third magnet ring that ends at the centerline of the magnet. Further interrogation of the area surrounding the cusp region will yield better insight into the sheath dimensions. In these experiments the centerline appears to line up with 0 mm on the position axis. The discrepancy between centerline position in the emissive and Langmuir probe experiments will be investigated further in future work.

By utilizing a simple center-differencing scheme, the x and y components of the electric field were calculated. Electric field magnitude in the cusp region is plotted for the low current case (Figure 19) and the high current case (Figure 20). In both cases the field magnitude appears to be approximately zero everywhere except for a high-field region along the cusp centerline. This line represents the edge of collection and thus a sharp drop in potential. The distinctive oval-shaped blips are due to noise in the data and are not expected to represent the actual electric field in the cusp.

## IV. Conclusion

Previous experiments studying the behavior of primary electrons in the cusp region of a multipole discharge chamber were expanded upon and refined by making use of a 3-axis motorized positioning system and automated data collection. The source was operated in the condition of zero gas flow such that the chamber was populated largely with primary electrons. A translatable Langmuir probe took current density measurements in the cusp region, and a translatable emissive probe took corresponding potential measurements. The data suggests there are primary electrons trapped at the ring cusp used as the target of these interrogations. These electrons are unable to cross over to the fourth ring due to a lack of collisions in the chamber. Integrating current over each interrogation track gave approximate primary electron transmission coefficients ranging from 0.18 to 0.58, with minimum transmission occurring at the low current case and transmission reaching a peak at moderate current levels.

Future work will involve running similar experiments in the case of gas flow, in which studies will be conducted analyzing the collection behavior of each particle species: ion, plasma electron, and primary electron. This will allow for the accounting of primary and secondary electron density and corresponding ionization rates. These experiments will also help determine just where the plasma is being produced. The current experiments will also be physically extended by investigating multiple magnet rings and interrogating further up towards the bulk region, perhaps even to the chamber centerline. In other words, a map will be created of the region bounded by the second and third magnet ring cusps in various levels of gas flow. The current discharge chamber will be modified to a cylindrical or planar geometry to allow for better access to the entire magnetic circuit. Once the effective loss area is established, modeling work can begin.

## References


[1]Bosch, R.A. and Merlino, R.L., "Confinement properties of a low-beta discharge in a spindle cusp magnetic field," *Phys. Fluids*, Vol. 29 No. 6, 1998-2006, 1986.

[2]Koch, C., and Matthieussent, M. "Collisional diffusion of a plasma in multipolar and picket fence devices." Phys. Fluids Vol. 26, No. 2 pp. 545-555. 1982.

[3]Horiike, H., Masato, A., Yoshihiro, O., Okumura, Y. and Tanaka, S., "Cusp width and power flow study at a high power magnetic multipole ion source," *Physics of Fluids*, Vol. 30, No. 10, pp. 3268-3275, 1987.

[4]Knorr, G., and Merlino, R.L., "The Role of Fast Electrons for the Confinement of Plasma by Magnetic Cusps," *Plasma Physics and Controlled Fusion*, Vol. 26, No. 2, 443-442, 1984.

[5]Pechacek, R.E. et al, "Measurement of plasma width in a ring cusp," *Physics Review Letters*, Vol. 45, No. 4, 256, 1980.

[6]Hwang, S.W., Lee, Y.J., Han, H.R., Yoo, J.B., Yeom, G.Y., "Effects of variously configured magnets on the characteristics of inductively coupled plasmas," *Journal of Vacuum Science and Technology A*, Vol. 17, No. 4, pp. 1211-1216, 1999.

[7]Morishita, T., Ogasawara, M., and Hatayama, A., "Estimate of cusp loss width in multicusp negative ion source," *Review of Scientific Instruments*, Vol. 69, No. 2, pp. 968-970, 1998.

[8]Goebel, D., "Ion source discharge performance and stability," *Physics of Fluids*, Vol. 25, No. 6, pp. 1093-1102, 1982.

[9]Anukaliani, A., and Selvarajan, V., "Loss of plasma scaling with magnetic field, pressure, and discharge current in a CUSP confined plasma," *The European Physical Journal Applied Physics*, Vol. 15 pp. 199-206, 2001.

[10]Kozima, H., Kawamoto, S., and Tamagiwa, K., "On the leak width of line and point cusp magnetic fields," *Physics Review Letters*, Vol. 86A, No. 6,7, 373, 1981.

[11]Arakawa, Y., and Hamatani, C., "Analysis of Plasma Loss in a Ring-Cusp Ion Thruster," Proceedings of the 19th International Electric Populsion Conference, Colorado Springs, AIAA Paper 87-1079, 1987.

[12]Limpaecher, R., and MacKenzie, K.R., "Magnetic Multipole Containment of Large Uniform Collisionless Quiescent Plasmas," *Review of Scientific Instruments*, Vol. 44, No. 6, 726-730, 1973.

[13]Gauthereau, C., and Matthieussent, G., "Plasma Density Profiles in Discharges Surrounded by Magnetic Multipole Walls," *Physics Letters*, Vol. 102a, No. 5,6, 231-234, 1984.

[14]Lagarde, T., Pelletier, J., and Arnal, Y., "Influence of the multipolar magnetic field configuration on the density of distributed electron cyclotron resonance plasmas," *Plasma Sources Science and Technology*, Vol. 6, pp. 53-60, 1997.

[15]Sandontano, G.M., Barroso, J.J., and Montes, A., "Magnetic Confinement Studies for Performance Enhancement of a 5-cm Ion Thruster," *IEEE Transactions on Plasma Science*, Vol. 24, No. 6, pp. 1319-1329, 1996.

[16]Wirz, R. and Goebel, D., "Ion Thruster Discharge Performance per Magnetic Field Topology," Proceedings of the 42nd AIAA/ASM/SAE/ASEE Joint Propulsion Conference, AIAA Paper 2006-4487, 2006.

[17]Goebel, D., Wirz, R., and Katz, I., "Analytical Ion Thruster Discharge Performance Model," *Journal of Propulsion and Power*, Vol. 23, No. 5, 1055-1067, 2007.

[18]Buzzi, J.M., Snow, J., and Hirshfield, J.L., "Primary Electron Reflections in Discharges Surrounded by Magnetic Multipole Walls," *Physics Letters*, Vol. 54A, No. 4, pp. 344-346, 1975.

[19]Hershkowitz, N., Leung, K.N., and Romesser, "Plasma Leakage Through a Low-Beta Line Cusp," *Physics Review Letters*, Vol. 35, No. 5, 227-280, 1975.

[20]Jones, R., "A source of error in cusp plasma leak measurements," *Plasma Physics*, Vol. 21, 505, 1979.

[21]Arakawa, Y. and Hamatani, C., "Reduction of Plasma loss to discharge chamber walls in a ring-cusp ion thruster," *Journal of Propulsion and Power*, Vol. 3, No. 1, 90, 1987.
[22]Sovey, J.S., "Improved Ion Containment Using a Ring-Cusp Ion Thruster," *Journal of Spacecraft*, Vol. 21, No. 5, 1983.
[23]Leung, K.N., Samec, T.K., and Lamm, A., "Optimization of Permanent Magnet Plasma Confinement," *Physics Letters*, Vol. 51A, No. 8, pp. 490-492, 1975.
[24]Sadowski, M., "Containment Time of Plasma in the SM Magnetic Trap," *Physics Letters*, Vol. 28A, No. 9, pp. 626-627, 1969.
[25]Hubble, A.A. and Foster, J.E., "Plasma collection width measurements in a 10-cm ring cusp discharge chamber," Proceedings of the 44th AIAA/ASM/SAE/ASEE Joint Propulsion Conference, Hartford, AIAA Paper 2008-4639, 2008.
[26]Wirz, R. and Goebel, D., "Effects of magnetic field topology on ion thruster discharge performance," *Plasma Sources Sci. Technol.* Vol. 17, 2008.
[27]Lieberman, M. and Lichtenberg, A., *Principles of Plasma Discharges and Materials Processing*, 2nd ed., John Wiley & Sons, New Jersey, 2005.
[28]Smith, J.R. Hershkowitz, N., and Coakley, P., "Inflection-point method of interpreting emissive probe characteristics," *Review of Scientific Instruments*, Vol. 50, No. 2, 210-218, 1979.
[29]Takekida, H., and Nanbu, K., "Particle modeling of plasma confinement by a multipolar magnetic field," *Jouranl of Physics D: Applied Physics*, Vol. 37, pp. 1800-1808, 2004.